Mem. S.A.It. Suppl. Vol. 18, 127

Memorie della
Supplementi

Global $m = 1$ instabilities and lopsidedness in disc galaxies

S. De Rijcke[1], V. Dury[1], V. P. Debattista[2], and H. Dejonghe[1]

[1] Sterrenkundig Observatorium, Universiteit Gent, Gent, Belgium
e-mail: Sven.DeRijcke@UGent.be
[2] Centre for Astrophysics, University of Central Lancashire, Preston, UK

Abstract. Lopsidedness is common in spiral galaxies. Often, there is no obvious external cause, such as an interaction with a nearby galaxy, for such features. Alternatively, the lopsidedness may have an internal cause, such as a dynamical instability. In order to explore this idea, we have developed a computer code that searches for self-consistent perturbations in razor-thin disc galaxies and performed a thorough mode-analysis of a suite of dynamical models for disc galaxies embedded in an inert dark matter halo with varying amounts of rotation and radial anisotropy.

Key words. galaxies: kinematics and dynamics – galaxies: spiral – galaxies: structure – instabilities

1. Introduction

The stellar and/or gaseous discs of spiral galaxies are often affected by large-scale asymmetries. About half of all late-type galaxies show a lopsided structure that affects the whole disc (Richter & Sancisi 1994; Haynes et al. 1998). Based on near-infrared images of a sample of 149 disc galaxies, Bournaud et al. (2005) find that a large fraction of them have asymmetric stellar discs. The strength of the lopsidedness does not correlate with the presence of companions but, instead, correlates with the presence of bars and spiral arms. Angiras et al. (2006) analysed HI surface density maps and R-band images of 18 galaxies in the Eridanus group. All galaxies showed significant lopsidedness in their HI discs. Where the stellar and gaseous discs overlap, their asymmetries are comparably strong. Since the Eridanus group galaxies are more strongly lopsided than field galaxies, these authors conclude that tidal interaction in the group environment may contribute to generating lopsidedness in disc galaxies. Lopsided structures are not the prerogative of disc galaxies alone. In some nucleated dwarf elliptical galaxies, for instance, the nucleus is displaced with respect to the centre of the outer isophotes (Bingelli et al. 2000). While some authors regard these displaced nuclei as being globular clusters projected close to the galaxy photocentre (Côté et al. 2006), in some cases, such as the Fornax dwarf elliptical FCC 046, there are clear indications that the nucleus is an integral part of the galaxy's stellar body and is displaced by a mechanism that affects the whole galaxy (De Rijcke & Debattista 2004).

Send offprint requests to: Sven De Rijcke

Here, we investigate the role played by instabilities in generating lopsidedness in isolated disc galaxies using a semi-analytic matrix method originally developed by Vauterin & Dejonghe (1996). More specifically, we explore whether lopsided instabilities can be triggered in fully rotating disc galaxies. The full details of this work can be found in Dury et al. (2008)

2. Searching for instabilities

We have developed a computer code to analyse the stability of razor-thin stellar discs embedded in an axisymmetric or spherical dark matter halo. The halo is assumed to be dynamically too hot to develop any instabilities. This inert halo only enters the calculations by its contribution to the global gravitational potential. We only consider the stellar component of the disc and neglect the dynamical influence of gas and dust.

We describe an instability as the superposition of a time-independent axisymmetric equilibrium configuration and a perturbation that is sufficiently small to warrant the linearization of the Boltzmann equation. The equilibrium configuration is characterized completely by the global potential $V_0(r)$ and the distribution function $f_0(E, J)$, with binding energy E and angular momentum J. A general perturbing potential can be expanded in a series of normal modes of the form

$$V'(r, \theta, t) = V'(r) e^{i(m\theta - \omega t)} \tag{1}$$

with a pattern speed $\Re(\omega)/m$ and growth rate $\Im(\omega)$ that, owing to the linearity of the relevant equations, can be studied independently from each other. The evolution of the perturbed part of the distribution function, denoted by $f'(\mathbf{r}, \mathbf{v}; t)$ can be calculated using the linearised collisionless Boltzmann equation

$$\frac{\partial f'}{\partial t} - [f', E] = [f_0, V']. \tag{2}$$

This equation can be readily integrated, yielding the concise form

$$f'(\mathbf{r}, \mathbf{v}; t) \; = \; e^{i(m\theta - \omega t)} \times \sum_{-\infty}^{\infty} I_l \frac{(l\omega_r + m\omega_\theta)\frac{\partial f_0}{\partial E} - m\frac{\partial f_0}{\partial J}}{l\omega_r + m\omega_\theta - \omega} e^{i(l\omega_r t(r) - m\theta_p(r))}. \tag{3}$$

The coefficients I_l come from the Fourier expansion of the ω_r-periodic part of the perturbing potential:

$$V'(r) e^{i(m\theta - \omega t)} \; = \; e^{i(m\omega_\theta - \omega)t} \sum_{-\infty}^{\infty} I_l e^{il\omega_r t}. \tag{4}$$

In order to calculate these coefficients, one needs to integrate the ω_r-periodic part of the perturbing potential along half a radial period of an unperturbed orbit. The radial coordinate r is then a periodic function of time with angular frequency ω_r, just like v_r and v_θ. Because the mean value of v_θ can be different from zero, θ will be the superposition of a periodic function $\theta_p(t)$ and a uniform drift velocity ω_θ:

$$\theta = \omega_\theta t + \theta_p(t). \tag{5}$$

Instead of using E and J, orbits in the unperturbed potential are catalogued by their apocentre and pericentre distances, denoted by r_+ and r_-, respectively. The sense of rotation is indicated by the sign of r_- . The grid of the orbit catalogue is given by $(r_+, r_-) \in [0, r_{max}] \times [-r_+, r_+]$. We use a grid of 100×200 cells. For every orbit, ω_r and ω_θ are determined, the Fourier expansion (4) is performed up to the order of $l_{\max} = 50$, and the coefficients are stored. If we want to calculate the response of the distribution function in the point $(\mathbf{r}, \mathbf{v}; t)$ in phase space at time t , we choose an orbit from the catalogue with the correct integrals of motion (i.e. r_+ and r_-) but passing through its apocentre at $t = 0$ so the actual orbit has an offset in time $t(r_0)$ and azimuth $\theta_p(r)$ that must be taken into account. Therefore, we also store a tabulation of $t(r)$ and $\theta_p(r)$.

3. The unperturbed models

The models we analysed all have the same gravitational potential and the same exponentially declining stellar surface density. The circular velocity curve is flat outside 1 kpc and both the disc and the halo are truncated at an outer limit of 6 kpc. The models are intended to mimic a small late-type disc galaxy. By varying the distribution function, we investigate the influence of the internal dynamics on the stability properties of the models. We

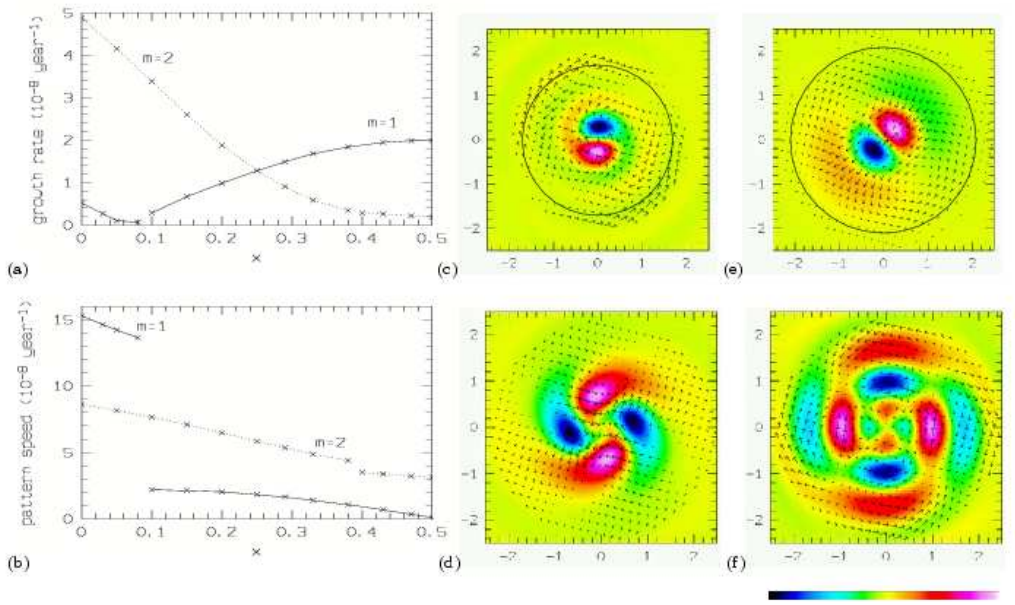

Fig. 1. Growth rate (a) and pattern speed (b) for the strongest $m = 1$ (solid line) and $m = 2$ (dotted line) instabilities as the fraction x of counter-rotating stars changes. Discontinuities appear when the nature of the instability changes. The perturbed density and velocity fields are plotted out to a radius of 2.5 kpc: (c) rotating one-armed spiral in the fully rotating model, (d) rotating two-armed spiral in the fully rotating model, (e) non-rotating lopsided mode in the counter-rotating model, and (f) one of a pair of counter-rotating bars in the counter-rotating model. Overdensities are coloured white/red, and underdensities black/blue. In panels (c) and (e), we also indicate the radius within which a growing $m = 1$ mode is expected based on density wave theory.

vary both the amount of net rotation, ranging between only prograde stars (a fully rotating disc) and equal numbers of prograde and retrograde stars (a counter-rotating disc), and the radial anisotropy.

4. The influence of rotation

In Fig. 1, we show the growth rates and pattern speeds of the fastest growing $m = 1$ and $m = 2$ modes as a function of the fraction x of retrograde stars. Clearly, the counter-rotating model has a dominant non-rotating $m = 1$ instability, whereas the $m = 2$ instability is virtually absent. As the degree of counter-rotation diminishes, the growth rate of the $m = 1$ instability slowly declines while it picks up a small pattern speed. At the same time, the $m = 2$ instability increases in strength. As long as more than one-quarter of all stars are on retrograde orbits, the model is dominated by a slowly rotating lopsided mode. Unexpectedly, around $x \approx 0.08$, the nature of the $m = 1$ mode changes: a rapidly rotating, lopsided instability becomes the fastest growing mode. Its strength increases together with that of the $m = 2$ mode as the degree of counter-rotation vanishes.

The dominant $m = 1$ mode we find in strongly counter-rotating models is obviously the well-known counter-rotation instability. This instability has been known since Zang & Hohl (1978) and has been studied analytically (Sawamura 1988; Palmer & Papaloizou 1990; Tremaine 2005) and using N-body simulations (Levison et al. 1990; Merritt & Stiavelli 1990; Sellwood & Merritt 1994; Sellwood & Valluri 1997). Partial rotation only introduces a pattern speed in an otherwise purely

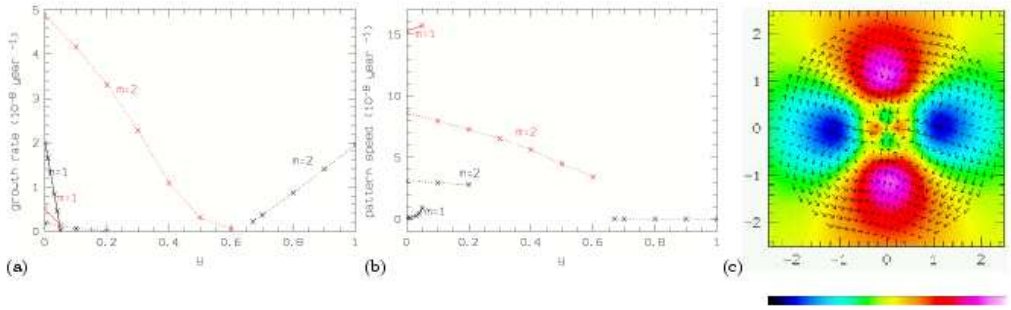

Fig. 2. Growth rate (a) and pattern speed (b) for the strongest $m = 1$ (solid line) and $m = 2$ (dotted line) instabilities as the fraction y of stars on radial orbits changes. The perturbed density and velocity field of the strongest $m = 2$ mode in a counter-rotating, strongly radially anisotropic model are shown in (c).

growing instability. The counter-rotating bars we found were also reported by Sellwood & Merritt (1994), Levison et al. (1990), and Friedli (1996). Sellwood & Valluri (1997) argued that they were the result of non-linear orbit trapping in finite-amplitude spiral disturbances. The fact that we found them shows that they are formed through linear instabilities.

The weaker $m = 1$ mode that we found in the rotating model has a certain sense of rotation and bears strong resemblance to the so-called eccentricity instability that occurs in gaseous and stellar near-Keplerian discs orbiting a central massive object (Adams et al. 1989; Shu et al. 1990; Noh et al. 1991; Taga & Iye 1998; Lovelace et al. 1999; Bacon et al. 2001; Jacobs & Sellwood 2001; Salow & Statler 2004). The first N-body example of a rotating lopsided instability was found by Sellwood (1985) in a mass model of our Galaxy without a halo component. Evans & Read (1998) examined the global stability of stellar power-law discs. They report a similar rotating lopsided pattern in cut-out power-law discs, but found no growing non-axisymmetric modes in the fully self-consistent power-law discs. We provide the first theoretical evidence that the eccentricity instability can also occur in the fully prograde stellar discs of spiral galaxies without an additional massive central component, such as a compact bulge or supermassive black hole, and without introducing an unresponsive central region in the disc.

5. The influence of radial anisotropy

In Fig. 2, we show the growth rates and pattern speeds of the fastest growing $m = 1$ and $m = 2$ modes as a function of the fraction y of stars on radial orbits. As y increases, the $m = 1$ and $m = 2$ instabilities rapidly stabilize. The lopsided mode is the first to stabilize. The counter-rotating model becomes fully stable against both $m = 1$ and $m = 2$ modes at $y \approx 0.2$. For $y \gtrsim 0.6$, the model develops a non-rotating bar instability that becomes stronger as radial anisotropy increases. The perturbed density and velocity field of the bar of a radially anisotropic counter-rotating model are shown in Fig. 2c.

In the fully rotating model, the $m = 1$ and $m = 2$ instabilities also stabilize with increasing anisotropy. The $m = 2$ instability is the last one to stabilize and the model becomes stable for $y \gtrsim 0.6$. From this exercise, it is clear that the mechanism that is responsible for triggering the lopsided mode in the counter-rotating model relies heavily on virtually all stars moving on near-circular orbits. Even a relatively small contribution of stars on radial orbits makes it impossible for the disc to develop the $m = 1$ mode.

6. Physical interpretation

In order to unravel the physics behind the two distinct $m = 1$ modes, we study the orbits of

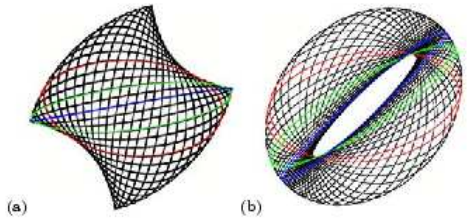

Fig. 3. Orbits in a lopsided potential : (a) butterfly orbit, (b) loop orbit.

stars that move in the global perturbed potential

$$V(r, \theta, t) = V_0(r) + \epsilon V'(r) e^{i(m\theta - \omega t)}. \quad (6)$$

In order to simplify the interpretation, we keep the amplitude of the perturbation fixed, that is, we set $\Im(\omega) = 0$ and only consider its pattern speed $\Re(\omega)/m$. The prefactor ϵ is determined by requiring that the maximum difference between the perturbed and the unperturbed density nowhere exceeds 10% of the unperturbed density. We then numerically evolve an ensemble of stars in the perturbed potential.

In the counter-rotating model, the $m = 1$ perturbation causes near-circular orbits to become somewhat more elliptic and to shift towards the slight overdensity. They become aligned loop orbits (see Fig. 3b), shifted in the direction of the overdensity. If the perturbation is strong enough, radial orbits become butterfly orbits (see Fig. 3b). A butterfly can be thought of as a librating ellipse orbit with varying ellipticity. As stars spend more time close to the apocenters of these librating ellipses, butterfly orbits tend to increase the stellar density in a direction perpendicular to the imposed $m = 1$ perturbation.

As shown in (Palmer 1994), a razor-thin disc consisting of two equal-mass counter-rotating stellar populations may develop purely growing one-armed ($m = 1$) Wentzel-Kramers-Brillouin (WKB) waves if the Toomre parameter, Q, fails to satisfy the local stability criterion

$$Q(r) \geq \frac{\kappa(r)^2}{\kappa(r)^2 - \Omega(r)^2}. \quad (7)$$

The precise form of this stability criterion depends on three approximations: (i) the WKB approximation for tightly wound spiral waves, (ii) the epicycle description for near-circular stellar orbits, and (iii) a Gaussian distribution function. None of these necessarily applies to the models presented in this paper. Nonetheless, we used the $Q(r)$, $\kappa(r)$, and $\Omega(r)$ profiles of the fully counter-rotating models, with varying radial anisotropy, to evaluate this criterion as a function of radius. We only check the fully counter-rotating models since only in this case can an analytical stability criterion be derived. The region where $m = 1$ waves can grow according to this criterion coincides with the region in which the lopsided mode resides according to our code (see Fig. 2e).

In the fully rotating model, the aligned loops also produce the main inner lobes of the $m = 1$ pattern. There is a stable Lagrange point on the corotation radius where stars tend to spend somewhat more time, causing the one-armed trailing spiral. In the non-linear regime, orbits can become trapped in resonance around this Lagrange point and become banana shaped in a reference frame that rotates with the same pattern speed as the perturbation.

The interpretation of this instability in terms of waves is somewhat subtle. In the case of a bar instability, the radial extent of the $m = 2$ pattern is determined by the largest radius out to which the most slowly rotating wave that avoids having an inner Lindblad resonance (ILR) can travel. This constraint sets the size of the resonance cavity within which the pattern can grow by swing amplification. However, one-armed waves do not have an ILR, irrespective of their pattern speed. The radial extent of the $m = 1$ pattern is set by the largest radius out to which non-rotating wave packets can travel. This radius is determined by the discs dispersion relation. We used the WKB dispersion relation together with the $Q(r)$, $\kappa(r)$, and $\Omega(r)$ profiles of the fully rotating model to estimate the region in which non-rotating one-armed waves are allowed to exist. The $Q(r)$ profile of the fully rotating model rises outwardly, limiting the extent of non-rotating waves to some finite radius, well within the disc. For a zero pattern speed, the dispersion

relation has two branches (the long-wave and the short-wave branch) of incoming and outgoing leading and trailing waves for radii smaller than approximately 1.7 kpc. This sets the dimension of the resonance cavity within which the pattern can grow through swing amplification. All $m = 1$ waves can propagate into the galaxy centre where incoming trailing wave packets are reflected as outgoing leading wave packets, closing the feedback loop. Moreover, a more steeply rising rotation curve will suppress the $m = 2$ mode while leaving the $m = 1$ mode, which has no ILR, largely intact. Thus, following Evans & Read (1998) who already proposed this mechanism as the cause of the $m = 1$ modes found in cut-out power-law discs, we propose swing amplification as the physical cause of the one-armed mode in this rotating model.

Acknowledgements. SDR is grateful to the Omega08 organizers for the opportunity to present this work at a most enjoyable workshop.

References

Angiras, R. A., Jog, C. A., Omar, A., & Dwarakanath, K. S. 2006, MNRAS, 369, 1849
Adams, F. C., Ruden, S. P., & Shu, F. H. 1989, ApJ, 347, 959
Bacon, R., Emsellem, E., Combes, F., et al. 2001, A&A, 371, 409
Binggeli, B., Barazza, F., & Jerjen, H., 2000 A&A, 359, 447
Bournaud, F., Combes, F., Jog, C. J., & Puerari, I. 2005, A&A, 438, 507
Côté, P., Piatek, S., Ferrarese, L., et al. 2006, ApJS, 165, 57
De Rijcke, S., & Debattista, V. P. 2004, ApJ, 603, L25
Dury V., De Rijcke S., Debattista, V. P., & Dejonghe, H. 2008, MNRAS, 387, 2
Evans, N. W., & Read, J. C. A. 1998, MNRAS, 300, 106
Friedli, D. 1996, A&A, 312, 761
Haynes, M. P., Hogg, D. E., Maddalena, R. J., Roberts, M. S., & van Zee, L. 1998, AJ, 304, 62
Jacobs, V., & Sellwood, J. A. 2001, ApJ, 555, L25
Levison, H. F., Duncan, M. J., & Smith, B. F. 1990, ApJ, 363, 66
Lovelace, R. V. E., Zhang, L., Kornreich, D. A., & Haynes, M. P. 1999, ApJ, 524, 634
Merritt, D., & Stiavelli, M. 1990, ApJ, 358, 399
Noh, H., Vishniac, E. T., & Cochran, W. D. 1991, ApJ, 383, 372
Palmer, P. L. 1994, Stability of Collisionless Stellar Systems (Kluwer, Dordrecht)
Palmer, P. L., & Papaloizou, J. 1990, MNRAS, 243, 263
Richter, O.-G., & Sancisi, R. 1994, A&A, 304, L9
Salow, R. M., & Statler, T. S. 2004, ApJ, 611, 245
Sawamura, M. 1988, PASJ, 40, 279
Sellwood, J. A. 1985, MNRAS, 217, 127
Sellwood, J. A., & Merritt, D. 1994, ApJ, 425, 530
Sellwood, J. A., & Valluri, M. 1997, MNRAS, 287, 124
Shu, F. H., Tremaine, S., Adams, F. C., & Ruden, S. P. 1990, ApJ, 358, 495
Taga, M., & Iye, M. 1998, MNRAS, 299, 1132
Tremaine, S. 2005, ApJ, 625, 143
Vauterin, P., & Dejonghe, H. 1996, A&A, 313, 465
Zang, T. A., & Hohl, F. 1978, ApJ, 226, 52